

PRESSURE SOURCE CONTRIBUTION AND NEAR WALL FLOW STRUCTURES RELATED TO HIGH AMPLITUDE WALL PRESSURE PEAKS

Yoshitsugu Naka

Department of Mechanical Engineering
Meiji University
1-1-1 Higashimita Tama-ku Kawasaki, Japan
email: naka@meiji.ac.jp

Kosuke Osawa

School of Aeronautics
Universidad Politécnica de Madrid
Plaza del Cardenal Cisneros 3, Madrid, Spain
email: kosawa@torroja.dmt.upm.es

ABSTRACT

Coherent flow structures contributing to high amplitude wall pressure peaks are identified using a direct numerical simulation (DNS) database of a turbulent channel flow. A new theoretical formulation for the local pressure source contribution is derived from the Poisson equation for pressure using the delta function. A high amplitude wall pressure peak is defined as a local maximum in magnitude larger than three times of the overall root mean square value. The high amplitude wall pressure peaks are mostly contributed from the near wall region up to the buffer layer for both positive and negative pressure peaks. The conditionally averaged flow fields around the high amplitude wall pressure peaks are evaluated. The spanwise asymmetry of the instantaneous flow field is carefully treated. The conditionally averaged field associated with the positive wall pressure peaks indicates the inclined streamwise vortices lining in the streamwise direction. The negative pressure peak is found located right under the inclined streamwise vortex. Clustering analyses highlight that the positive high amplitude wall pressure peaks are related to multiple vortices in different positions. The wall pressure peaks are active in the large-scale high-speed region indicating a link between the high amplitude wall pressure peaks and the large-scale structures.

INTRODUCTION

Wall pressure fluctuations are like footprints of near wall turbulent flow structures. Johansson et al. (1987) showed that the positive high amplitude wall pressure peak is associated with a strong shear layer near the wall, while the negative high amplitude wall pressure peak is related to sweeps. Ghaemi and Scarano (2013) clarified the three-dimensional flow structure linked to high amplitude wall pressure peaks by conditional averaging. They showed that the positive pressure peak is relevant to the shear layer induced by the upstream sweep and the downstream ejection. It is also shown that the sweep motion originates from the outer layer and the ejection is caused by the hairpin vortex structure. Ghaemi and Scarano (2013) also mentioned that the negative pressure peak can be associated with the streamwise and spanwise vortices. Mehrez et al. (2019) visualized the turbulence structure associated with the wall pressure fluctuation using the second invariant of the velocity gradient tensor, and showed that the peak of the fluctuating pressure is linked to the turbulent structure in both inner and outer layers. Although the vortex structure related to the fluctuating wall pressure obtained by their conditional averaging exhibits a hairpin-like shape, the location and size of the structure are different from the typical hairpin vortex structure model proposed by Adrian et al. (2000).

The present study aims to clarify the relation between the wall pressure fluctuations and the turbulent flow structures in the turbulent channel flow. Our interest lies in the local source contribution to the wall pressure fluctuation, which is evaluated from the spatial distribution of the contribution to the wall pressure at a certain point based on the Poisson equation of pressure. Appropriate statistical procedures will also be applied to reveal the characteristics of the flow field associated with high amplitude wall pressure peaks.

CHANNEL FLOW DNS DATABASE AND FORMULATION OF LOCAL WALL PRESSURE CONTRIBUTION

The turbulent channel flow database for $Re_\tau = 178$ and 360 were established. To obtain the data of fully developed turbulent channel flows, direct numerical simulations (DNS) were performed using Incompact3D (Laizet and Lamballais, 2009). The computational conditions are summarized in Table 1. The computational parameters, i.e., the domain size and the grid resolution, were determined as in existing studies. The present results were validated against the existing DNS database (Del Alamo and Jiménez, 2003), and it was confirmed that the average velocity, the RMS value of velocity fluctuations, and the power spectrum are in good agreement.

The pressure field is obtained by separately solving the Poisson equation for pressure. Since the turbulent channel flow is periodic in the streamwise and spanwise directions, it is reasonable to use the Fourier transformed form of the Poisson equation as in Kim (1989),

$$\hat{p}_w(\mathbf{k}) = \int 2\hat{Q}(y', \mathbf{k})\hat{G}_w(y', \mathbf{k}) dy' \quad (1)$$

where \hat{p}_w , \hat{G}_w and \hat{Q} are the wall pressure in the wave number space with the wave number \mathbf{k} , the Green's function, and the second invariant of the velocity gradient tensor, respectively. y' stands for the wall normal coordinate. A pressure source contribution at a location \mathbf{x}_o to the wall pressure at a point \mathbf{x} is represented by the delta function, and substituted it into Eq. (1) yields the local source contribution to the wall pressure as follows

$$\delta p_x(\mathbf{x}_o) = Q(\mathbf{x}_o)\tilde{G}(\mathbf{x}, \mathbf{x}_o) \quad (2)$$

where $\delta p_x(\mathbf{x}_o)$ expresses the contribution to the wall pressure at \mathbf{x} from the source at \mathbf{x}_o , and hereafter $\delta p_x(\mathbf{x}_o)$ is called the local pressure contribution. $Q(\mathbf{x}_o)$ indicates the second invariant of

Table 1. Computational parameters.

Re_τ	L_x	L_y	L_z	N_x	N_y	N_z
180	4π	2	$4\pi/3$	256	129	128
400	4π	2	$4\pi/3$	288	287	180

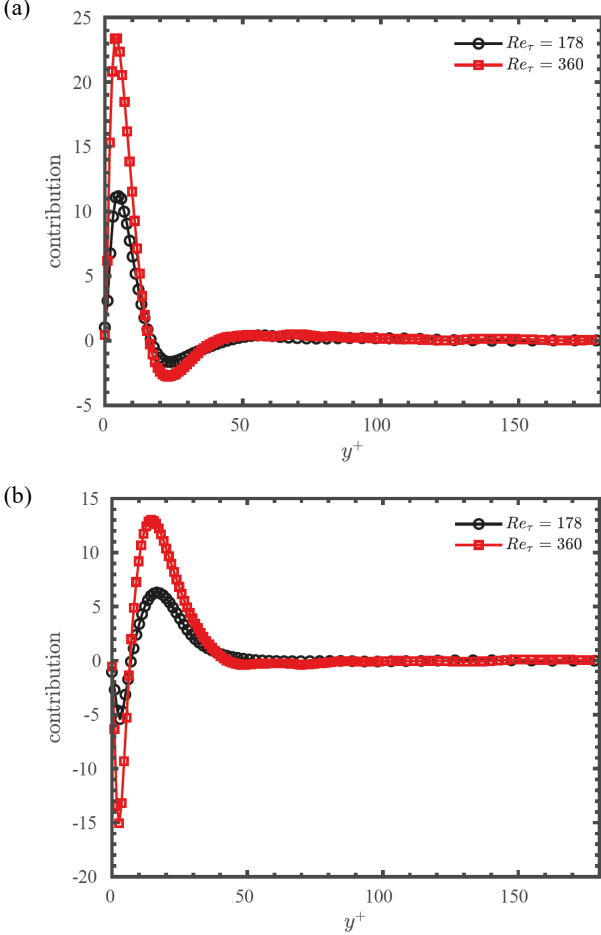


Figure 1. Wall normal profiles of averaged local contribution to the wall pressure fluctuation (a) for p_{\max} and (b) for p_{\min} .

the velocity gradient tensor at \mathbf{x}_o in the physical space, and $\tilde{G}(\mathbf{x}, \mathbf{x}_o)$ is the representation of the Green's function in physical space. One can evaluate the local pressure contribution using Eq. (2). It is noted that \tilde{G} at $\mathbf{x} \approx \mathbf{x}_o$ is negative, thus positive Q usually gives negative contribution to \hat{p}_w and vice versa.

AVERAGE SOURCE CONTRIBUTION AND TURBULENCE STRUCTURES ASSOCIATED WITH HIGH AMPLITUDE WALL PRESSURE PEAKS

The wall pressure maxima and minima, p_{\max} and p_{\min} , having magnitudes greater than three times of the RMS value of the overall wall pressure fluctuation, p_{rms} , are considered for the present analysis. Figure 1(a) and 1(b) show the wall normal distribution of the local pressure contribution to p_{\max} and p_{\min} averaged in the x - z plane, respectively. For the present Reynolds number range, the local pressure contributions are significant in

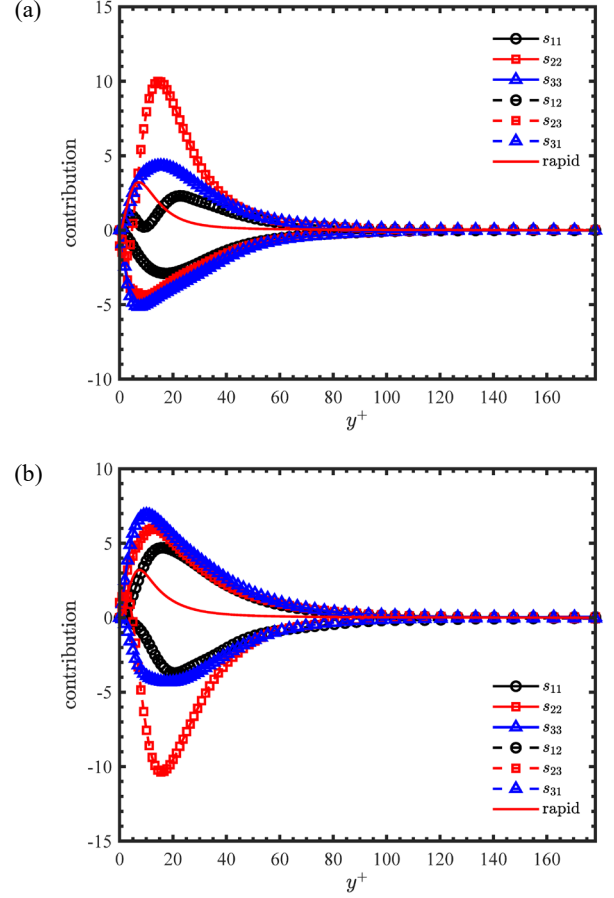


Figure 2. Contribution of rapid (line) and slow terms s_{ij} (a) for p_{\max} and (b) for p_{\min} . $Re_\tau = 180$.

the buffer layer. The contribution to p_{\max} shows a maximum at $y^+ = 5$ and minimum at $y^+ = 25$. Here, superscript “+” indicate the wall unit. On the other hand, the contribution to p_{\min} indicates a minimum at $y^+ = 5$ and a maximum around $y^+ = 15$.

The pressure source can be decomposed to the rapid term $\partial_y U \partial_x v$ and the slow terms $s_{ij} = \partial_j u_i \partial_i u_j$. Figures 2(a) and 2(b) show the contributions of these components on p_{\max} and p_{\min} , respectively. The rapid term works positive to p_{\max} , which means that $\partial_x v$ around p_{\max} is positive since $\partial_y U$ is positive. For p_{\min} , the rapid term is negative, that means $\partial_x v$ negative. In fact, Naka et al. (2015) reported that the positive wall pressure is correlated with the sweep ($u > 0$ and $v < 0$) at upstream; the negative wall pressure with the downstream sweep. Among the slow terms, the diagonal components, $(\partial_j u_j)^2$, contribute positive to the pressure by definition. Thus, they work positive for p_{\max} and negative for p_{\min} . On the other hand, the off-diagonal components generally contribute in opposite. s_{22} is the largest in magnitude while it turns to be positive in $y^+ < 3$. A noteworthy thing is that gradients in y and z have higher magnitude than that in x . For example, the magnitudes of s_{22} and s_{33} are larger than that of s_{11} , and s_{23} is larger than s_{12} and s_{31} . This suggest that the pressure peaks are associated with the structures elongated in the streamwise direction. The other thing to note is that all the terms exhibit peak within the buffer layer, up to $y^+ \approx 20$.

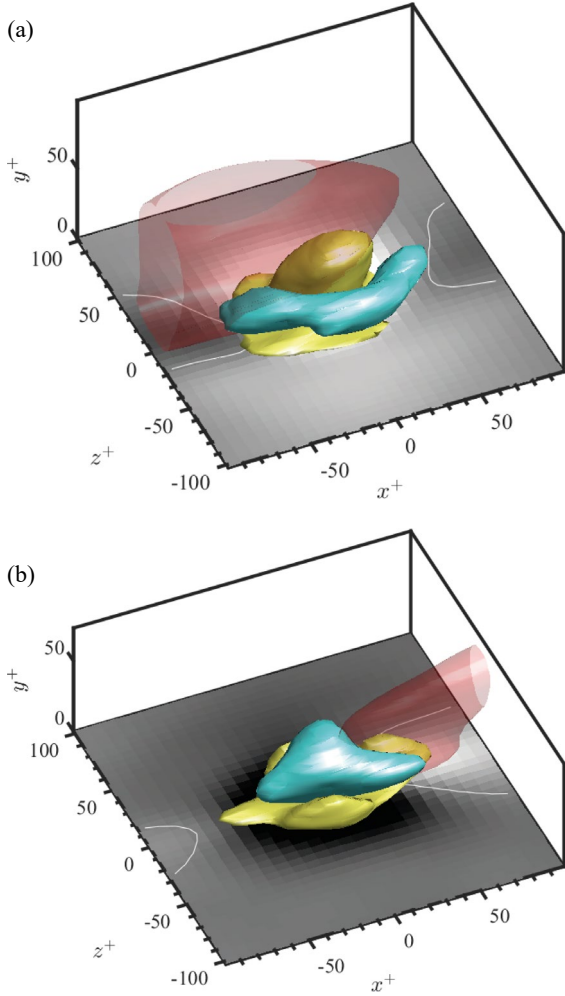


Figure 3. Conditionally averaged distribution around the high amplitude wall pressure peaks (a) for p_{\max} and (b) for p_{\min} . Yellow: $\delta p = \text{rms}(\delta p)$; cyan: $\delta p = -\text{rms}(\delta p)$; red: $u = u_\tau$. Bottom wall: p_w (darker to brighter), and contour at $p_w = 0$ (white line). $Re_\tau = 360$.

Figures 3(a) and 3(b) show the conditionally averaged distributions around p_{\max} and p_{\min} , respectively. To account for the asymmetry of the flow field in the spanwise direction, the orientation of the individual flow fields was aligned based on the distribution of Q so that the spatial averaged value of Q for subdomain in $z' < 0$ has larger than that for the subdomain in $z' > 0$, where z' is the spanwise coordinate after the alignment. From the region where $\delta p < 0$ (approximately corresponding to the region where $Q > 0$), the flow pattern associated with p_{\max} is reminiscent of longitudinal vortex structures tilted toward the flow direction. These longitudinal vortices are located slightly away from the pressure peak and surround the positive local pressure contribution. In contrast, for p_{\min} , the negative pressure contribution exists directly above the negative peak location. The characteristic shape of the negative pressure contribution seems to be decomposed to an elongated structure in the streamwise direction and a rather rounded shape region near the origin. For the elongated structure in the streamwise direction, it is similar to the longitudinal vortex structure observed in the distribution for p_{\max} . Ghaemi and Scarano (2013) pointed out that a spanwise vortex structure is observed just above the

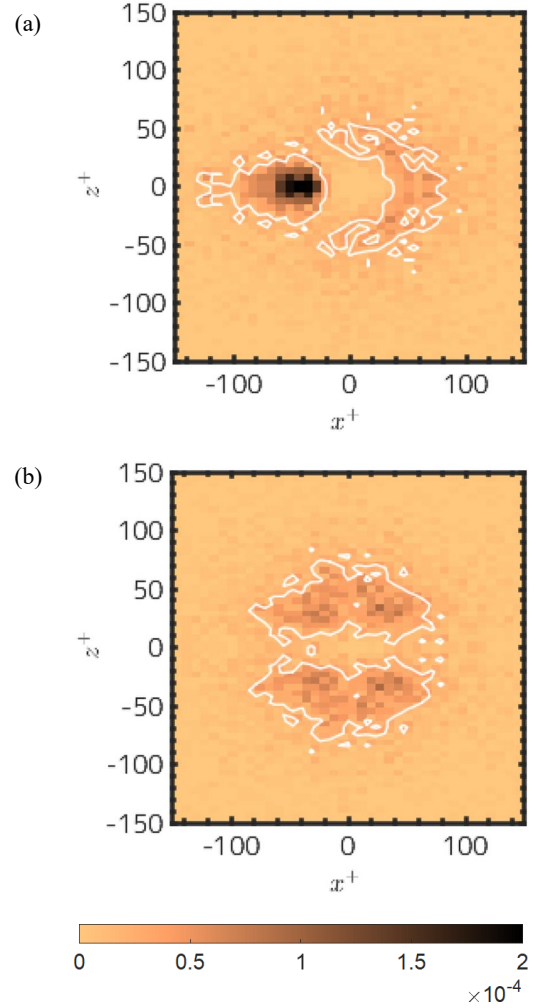


Figure 4. Probability density functions of the relative position from an intense pressure peak to the closest peak. Area within white line contains 50% of data; (a) p_{\min} around p_{\max} , (b) p_{\max} around p_{\max} . $Re_\tau = 360$.

negative pressure peak, and that this corresponds to the head of the hairpin vortex. In the present study, although the significant negative contribution region of a round shape is found just above the peak, no clear hairpin-like structure is observed. This suggests that different coherent structures can be extracted by different averaging procedures.

It is found that p_{\max} and p_{\min} are respectively located at the front and back of the sweep motion, which is indicated by the red transparent iso-surface in Fig. 3. Furthermore, the mean wall pressure changes its sign in the streamwise direction with the spacing of $\Delta x^+ \approx \pm 75$. This suggests that the positive and negative peaks form a pair.

PAIRING CHARACTERISTICS OF POSITIVE AND NEGATIVE WALL PRESSURE PEAKS

The conditionally averaged flow distributions presented in Fig. 3 suggest that p_{\max} and p_{\min} are likely to be associated with streamwise vortices aligned in the streamwise direction. The pairing characteristics of p_{\min} and p_{\max} are investigated. For each pressure peak, the closest peak with the opposite sign

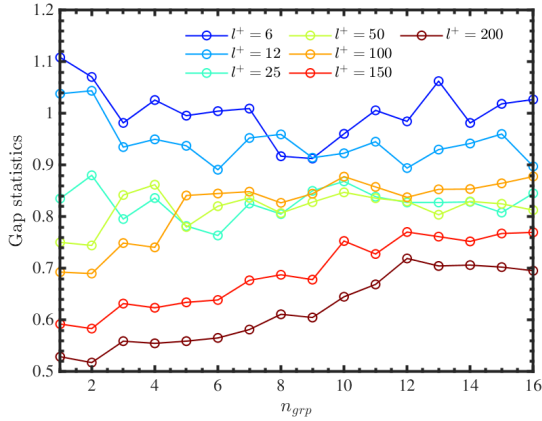


Figure 5. Behaviour of gap statistics against the number of clusters, n_{grp} with different filter widths.

is extracted. Figure 4 shows probability density function (PDF) of the relative positions of such pairs. Two combinations of the pressure peaks are considered: p_{min} around p_{max} shown in Fig. 4(a), and p_{max} around p_{max} in Fig. 4(b). Figure 4(a) indicates that p_{max} tend to have p_{min} at 50^+ in upstream. Although this distance is somewhat shorter than the distance measured from the conditional average, 75^+ , shown in Fig. 3(a), they coincide well when considering the difference of the instantaneous peaks and the peaks in the averaged wall pressure. These results confirm that the pressure peaks form a pair in the streamwise direction in the instantaneous distribution.

The PDF of p_{max} around p_{max} , shown in Fig. 4(b), has a peak in the spanwise direction, although these peaks are less clear compared to those of $p_{min} - p_{max}$ pairs. The most probable distance is $25^+ - 30^+$, and therefore the pressure peaks can be associated with streamwise elongated structure in the buffer layer.

CLUSTERING ANALYSES OF SOURCE DISTRIBUTION ASSOCIATED WITH POSITIVE WALL PRESSURE PEAKS

In the previous section, the representative flow pattern is extracted based on the conditional sampling taking into account of asymmetry of the flow in the spanwise direction. When defining the representative flow structure associated with a flow event, we are in a dilemma that averaging smears out instantaneous features, and a subjectively chosen instantaneous snapshot cannot represent the whole phenomena. To overcome such a situation and to further investigate the representative structures of the source distributions contributing to the pressure peaks, the clustering analyses are introduced. The clustering analysis is widely used to separate data into groups (Hastie et al., 2009) based on the pairwise distance. Here, the source distributions around p_{max} are served for the K-means clustering analysis. When p_{max} can be associated with some representative distribution patterns, it is expected that they are grouped to different clusters.

When performing the K-means clustering, one should specify the number of clusters, k , as an input parameter while it is not known a priori. The behaviour of the sum of the pairwise distance of each cluster gives a hint to choose a good value of k , and there is a common practice so-called ‘‘the elbow method’’

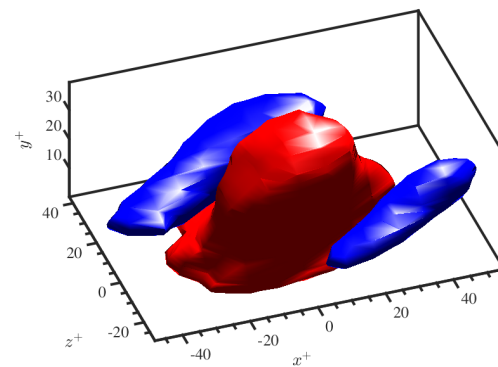
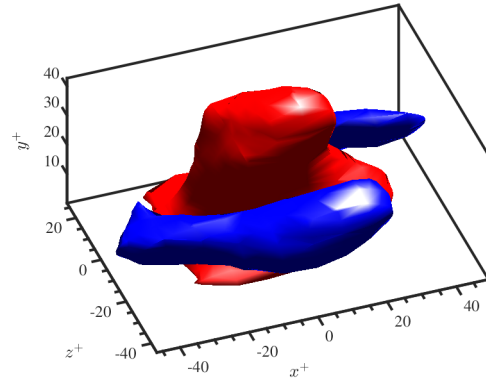
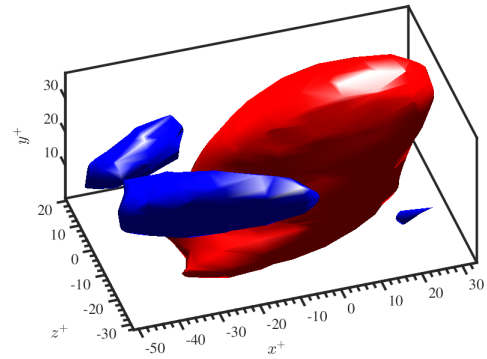
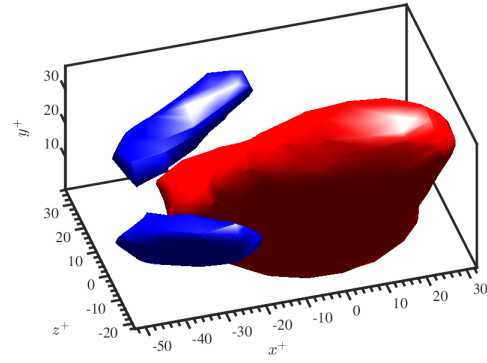


Figure 6. Representative structures around p_{max} identified by the K-means clustering: the ensemble average of each cluster. The red and blue isosurfaces indicate the intense positive and negative local pressure contributions.

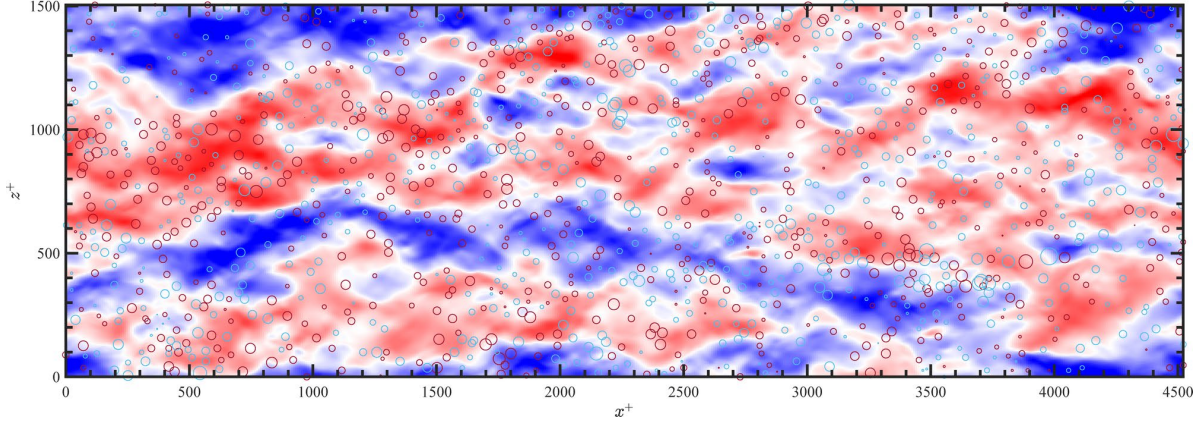


Figure 7. Streamwise velocity averaged over $y^+ \geq 100$ (colormap) with p_{\max} (red circle) and p_{\min} (blue circle). Size of circle is proportional to the magnitude of pressure peaks. $Re_\tau = 400$.

finding a point ending the rapid decrease of the sum of distance. The gap statistic (Tibshirani et al., 2001) is a quantitative measure for reasonable determination of the number of clusters. The gap value is defined as the logarithmic ratio of the sum of the pairwise distance of reference data over that of the served data. The reference data are white noise having the uniform distribution along with the data axes or along with the principal component axes of the data. When the sum of the distance of the served data is significantly smaller than the reference, it gives the large gap value. The behaviour of the gap value for different number of clusters facilitates a reasonable determination of k .

In the present study, instead of the white noise reference, randomly sampled data in the flow field are used. Reference data are taken in the same way as the data around p_{\max} but they are taken at randomly sampled points. This can highlight the meaningful cluster of the data around p_{\max} against the background wall pressure fluctuations. The positive gap value indicates the sum of the distance for p_{\max} is smaller than that of the randomly sampled data, which means the data of p_{\max} are meaningfully clustered.

The data are filtered in space before being served for the clustering so that the data can contain a certain size of the structures with a smaller number of dimensions. Here, the number of dimensions is fixed to 8, i.e., $2 \times 2 \times 2$ in space, and the different filter widths are tested. In x and z directions, the boxes are defined in the negative and positive regions, and in y direction, the box in the near wall region, $0 \leq y^+ \leq 15$, and the box further from the wall, $y^+ > 15$, where the overall contribution changes its sign as presented in Fig. 1, are used. The number of samples is 13901. Figure 5 presents the behaviour of the gap values with different filter widths in x and z directions. The gap values are higher for smaller filter widths. The three groups are observed for small ($l^+ \leq 12$), medium ($25 \leq l^+ \leq 100$) and large ($150 \leq l^+ \leq 200$) filter widths, where l^+ denotes the filter width in the wall unit length. This suggests that the features detected with the filter width of $25^+ - 100^+$ play a specific role in clustering.

Figure 6 shows the ensemble average of the source distribution among the samples belonging to the same cluster. The clustering is performed with the filter width $l^+ = 100$. All clusters have positive source near the origin, which directly contributes to p_{\max} . For the different clusters, the negative contribution exists around the origin at different quadrants. The level of the iso-surface is set to visualize the intense local source

contribution corresponding to 150% of the RMS value of source within a box of dimension $200^+ \times 100^+ \times 200^+$. Figure 6 indicates that p_{\max} is primarily associated with a strong inclined streamwise vortex, and weaker vortices co-exist around the primary one. The strong vortex (or vortices) induces the intense shear layer structure at $z = 0$ plane, which is often associated with positive wall pressure in the literature (Johansson et al., 1989; Ghaemi and Scarano, 2013; Mehrez et al., 2019).

AMPLIFICATION OF WALL PRESSURE PEAKS WITH LARGER SCALE STRUCTURES

Although our results show that the pressure peak is decided by the near-wall events beneath the buffer layer, Naka et al. (2015) and Gibeau and Ghaemi (2021) observed the association of the large-scale velocity structure. Figure 7 shows that the streamwise velocity averaged in the wall normal direction in the slab of $y^+ \geq 100$, hereafter denoted as u_{slab} , which is a proxy of the large-scale motion (LSM) in the outer layer. The intense pressure peaks overlaid in the figure with circles show preferential amplification in the high momentum side, e.g., $x^+ \approx 500$, $z^+ \approx 800$. Figure 8(a) shows the PDF of the u_{slab} above the pressure peaks. The pressure peaks more intense than $3p_{\text{rms}}$ tend to be located under the high momentum region, and the preferential amplification is evident. Figure 8(b) shows the same PDF but for the velocity in the near-wall slab of $0 \leq y^+ \leq 30$. It gives the consistent result as the far-wall slab, suggesting that the associated LSM is attached to the wall. As in Figs. 7 and 8, p_{\max} and p_{\min} are observed more in the large-scale high-speed region. It is noticeable that the intense peaks are located in the center part of the high-speed region as well as the interface between the high-speed and the low-speed regions. It also suggests that these wall pressure peaks are not directly linked to the hairpin packets which tend to exist around the low-speed region.

Though the positive and negative high amplitude pressure peaks are mostly contributed from the near wall region, i.e., up to the buffer layer, it is known that the characteristics of the wall pressure fluctuation cannot be scaled only with the near wall quantity (Tsuiji et al., 2007). The contribution of large-scale structure attached to the wall is evident. Such structures extend further from the wall and they consist of the large-scale and very large-scale motions. The large-scale motion itself can create large scale wall pressure but not small-scale high amplitude

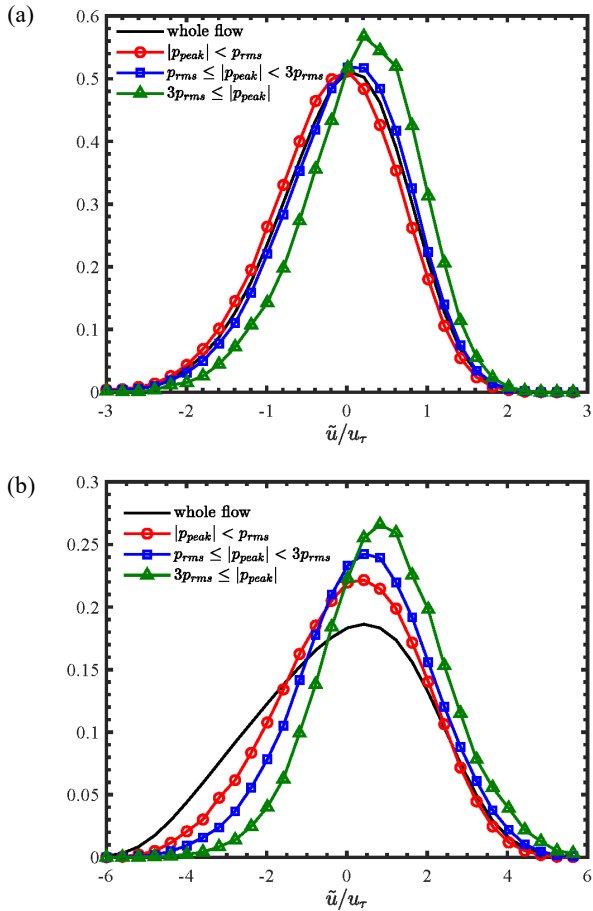


Figure 8. PDFs of the streamwise velocity conditioned on the magnitude of the pressure peaks. The velocity data above the pressure peak locations are sampled; (a) $y^+ \geq 100$ and (b) $0 \leq y^+ \leq 30$. $Re_\tau = 400$.

peaks. Even though the high amplitude pressure peaks are not directly contributed by the structures far from the wall, they can be correlated since the large-scale structure is wall attached and it extends further from the wall. This can be confirmed by the conditionally averaged flow pattern. The conditionally averaged velocity distribution shows meaningful sweep motion in the region higher than the channel half height.

CONCLUSION

The near wall turbulent flow structures related to the high amplitude wall pressure peaks are clarified using DNS data of a turbulent channel flow. The local pressure contribution is derived from the source term of the Poisson equation for pressure using the delta function. It is shown that most of the contribution to the high amplitude wall pressure peak is found in and below the buffer layer. The conditionally averaged flow fields around the high amplitude wall pressure peaks are evaluated. It is found that the extracted turbulent flow structure around the positive wall pressure peak is a longitudinal vortex structure surrounding the pressure peak position, and that of the negative wall pressure peak is a longitudinal vortex structure directly above the peak position. The positive and negative pressure peaks prone to conform pairs. The clustering analyses

highlight the representative turbulent flow structures having a single vortex or multiple vortices around positive wall pressure peaks. The pressure peaks tend to exist more under the large-scale high-speed region. It suggests that the high amplitude wall pressure peaks are indirectly enhanced in the large-scale high-speed region.

ACKNOWLEDGEMENT

This work was supported by JSPS KAKENHI Grant Number 19K04176.

REFERENCE

- Adrian, R. J., Meinhart, C. D., and Tomkins, C. D., 2000, "Vortex organization in the outer region of the turbulent boundary layer" *Journal of Fluid Mechanics*, Vol. 422, pp. 1-54.
- Del Alamo, J. C., and Jiménez, J., 2003, "Spectra of the very large anisotropic scales in turbulent channels", *Physics of Fluids*, Vol. 15, L41.
- Ghaemi, S., and Scarano, F., 2013, "Turbulent structure of high-amplitude pressure peaks within the turbulent boundary layer", *Journal of Fluid Mechanics*, Vol. 735, pp. 381-426.
- Gibeau, B. and Ghaemi, S., 2021, "Low- and mid-frequency wall-pressure sources in a turbulent boundary layer", *Journal of Fluid Mechanics* Vol. 918, A18.
- Hastie, T., Tibshirani, R. and Friedman, J. H., 2009, "The elements of statistical learning: data mining, inference, and prediction", Vol. 2, pp. 1-758, *Springer*.
- Johansson, A. V., Her, J.-Y., and Haritonidis, J. H., 1987, "On the generation of high-amplitude wall-pressure peaks in turbulent boundary layers and spots", *Journal of Fluid Mechanics*, Vol. 175, pp. 119-142.
- Kim, J., 1989, "On the structure of pressure fluctuations in simulated turbulent channel flow", *Journal of Fluid Mechanics*, Vol. 205, pp. 421-451.
- Laizet S., and Lamballais E., 2009, "High-order compact schemes for incompressible flows: a simple and efficient method with the quasi-spectral accuracy", *Journal Computational Physics*, Vol. 228, pp. 5989-6015.
- Mehrez, A., Yamamoto, Y., and Tsuji, Y., 2019, "Reynolds number dependence of turbulent structures associated with high-amplitude wall pressure peaks in channel flow", *Fluid Dynamics Research*, Vol. 51, 011407.
- Naka, Y., Stanislas, M., Foucaut, J.-M., Coudert, S., Laval, J.-P., and Obi, S., 2015, "Space-time pressure-velocity correlations in a turbulent boundary layer", *Journal of Fluid Mechanics*, Vol. 771, pp. 624-675.
- Tibshirani, R., Walther, G., & Hastie, T., 2001, "Estimating the number of clusters in a data set via the gap statistic", *Journal of the Royal Statistical Society: Series B (Statistical Methodology)*, Vol. 63, pp. 411-423.
- Tsuji, Y., Fransson, J. H. M., Alfredsson, P. H. & Johansson, A. V., 2007, "Pressure statistics and their scaling in high-Reynolds-number turbulent boundary layers", *Journal of Fluid Mechanics*, Vol. 585, pp. 1-40.